Modelling Viscosity of Volcanic Melts with Artificial Neural Networks

Dominic Langhammer[1,1,1], Gerd Steinle-Neumann[1,1,1], and Danilo Di Genova[2,2,2]

[1]Universität Bayreuth
[2]University of Bayreuth

November 30, 2022

Abstract

Viscosity is of great importance in governing the dynamics of volcanoes, including their eruptive style. The viscosity of a volcanic melt is dominated by temperature and chemical composition, both oxides and water content. The changes in melt structure resulting from the interactions between the various chemical components are complex, and the construction of a physical viscosity model that depends on composition has not yet been achieved. We therefore train an Artificial Neural Networks (ANN) on a large database of measured compositions, including water, and viscosities that spans virtually the entire chemical space of terrestrial magmas, as well as some technical and extraterrestrial silicate melts. The ANN uses composition, temperature, a structural parameter reflecting melt polymerisation and the alkaline ratio as input parameters. It successfully reproduces and predicts measurements in the database with significantly higher accuracy than previous global models for volcanic melt viscosities. A calculator based on our ANN model is available at https://share.streamlit.io/domlang/visc_calc/main/final_script.py. Viscosity measurements are restricted to low and high viscosity range, which exclude typical eruptive temperatures. Without training data at such conditions, the ANN cannot reliably predict viscosities for this important temperature range. To overcome this limitation, we use the ANN to create a synthetic viscosity data in the high and low viscosity regime and fit these points using a physically motivated, temperature-dependent viscosity model. An Excel file to calculate viscosities using these parameters and the MYEGA equation is supplied in the Supporting Information.

Modelling Viscosity of Volcanic Melts with Artificial Neural Networks

D. Langhammer[1], D. Di Genova[1], G. Steinle-Neumann[1]

[1]Bayerisches Geoinstitut, Universität Bayreuth, 95440 Bayreuth, Germany

Key Points:

- We train an Artificial Neural Network that calculates temperature- and composition-dependent viscosity of volcanic melts
- The Neural Network reproduces and predicts experimental viscosity significantly better than previous global models
- A synthetic data approach based on the Neural Network is combined with a physical model to predict viscosity at eruptive temperatures

Corresponding author: Dominic Langhammer, dominic.langhammer@uni-bayreuth.de

Abstract

Viscosity is of great importance in governing the dynamics of volcanoes, including their eruptive style. The viscosity of a volcanic melt is dominated by temperature and chemical composition, both oxides and water content. The changes in melt structure resulting from the interactions between the various chemical components are complex, and the construction of a physical viscosity model that depends on composition has not yet been achieved. We therefore train an Artificial Neural Networks (ANN) on a large database of measured compositions, including water, and viscosities that spans virtually the entire chemical space of terrestrial magmas, as well as some technical and extraterrestrial silicate melts. The ANN uses composition, temperature, a structural parameter reflecting melt polymerisation and the alkaline ratio as input parameters. It successfully reproduces and predicts measurements in the database with significantly higher accuracy than previous global models for volcanic melt viscosities. A calculator based on our ANN model is available at `https://share.streamlit.io/domlang/visc_calc/main/final_script.py`. Viscosity measurements are restricted to low and high viscosity range, which exclude typical eruptive temperatures. Without training data at such conditions, the ANN cannot reliably predict viscosities for this important temperature range. To overcome this limitation, we use the ANN to create a synthetic viscosity data in the high and low viscosity regime and fit these points using a physically motivated, temperature-dependent viscosity model. An Excel file to calculate viscosities using these parameters and the MYEGA equation is supplied in the Supporting Information.

Plain Language Summary

Magma viscosity is a key parameter that controls the style of a volcanic eruption, whether it will be effusive or explosive. For this reason, any volcanic hazard mitigation plan requires detailed knowledge of this property. Melt viscosity can vary by up to 15 orders of magnitude (a factor of a quadrillion) with temperature and composition. Unfortunately, it is not possible to perform measurements over this range continuously in the laboratory, but only in two distinct temperature regimes, termed high and low viscosity ranges. In order to obtain a model to predict how composition and temperature control viscosity, we use machine learning and train an artificial neural network on a large viscosity database. This allows us to calculate high- and low-temperature viscosity data that we call synthetic. Since most magmas are erupted at temperatures between the high and low-temperature ranges, we combine the synthetic data and a physically motivated equation to describe the dependence of viscosity on temperature. This model can compute viscosities in the region without measurements, including typical eruption temperatures of volcanoes. Our model serves the scientific community studying volcanic eruption mechanisms and its future prediction on a data driven basis.

1 Introduction

The shear viscosity (η) of volcanic melts is of great importance for the transport dynamics of magmas and the eruptive styles of volcanoes (Cassidy et al., 2018; Colucci & Papale, 2021; Di Genova et al., 2017a; Dingwell, 1996; Gonnermann & Manga, 2007; Papale, 1999), making η an important quantity for physical volcanology. Melt viscosity depends dominantly on chemical composition (x) and temperature (T). Previous work has often used a T-dependent expression to fit data from η measurements to a specific anhydrous composition. Common examples are the VFT (Fulcher, 1925; Tammann & Hesse, 1926; Vogel, 1921) and MYEGA (Mauro et al., 2009) models. With a critical influence of water on eruption dynamics (Gonnermann & Manga, 2013) and its strong control on viscosity, the dependence of η on H_2O is often considered separately in models. Such models are typically built by empirical modifications of the fitting parameters to include H_2O dependence (e.g., Dingwell et al., 1998; Giordano et al., 2009; Langham-

mer et al., 2021; Misiti et al., 2011; Robert et al., 2015; Vetere et al., 2006; Whittington, Hellwig, et al., 2009).

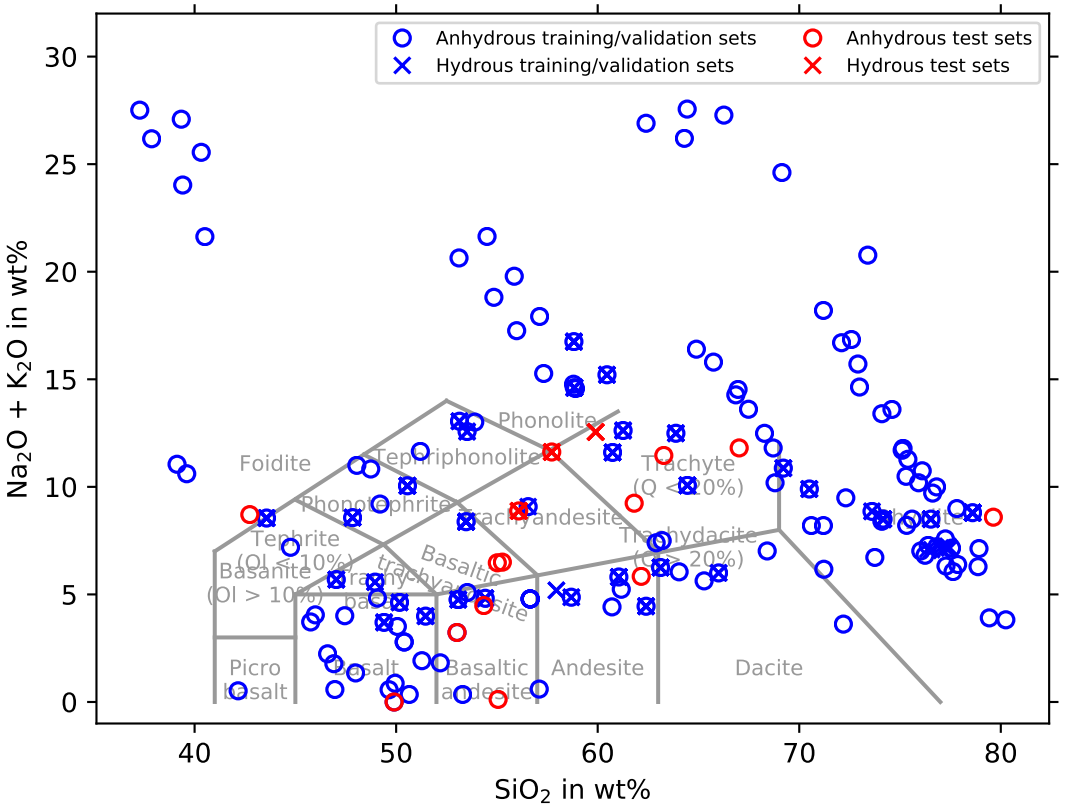

Figure 1. Total alkaline and silica content (Le Bas et al., 1986) for all data set in the database. Blue symbols indicate training/validation data sets and red symbols the test sets. Anhydrous data sets are shown by circles and hydrous by crosses. Values and references for the training/validation sets are given in Table 1 and for the test sets in Table 2.

In contrast to the individual melt fits, global models predict viscosity based on x, T (Giordano et al., 2008; Hui & Zhang, 2007) and pressure P (Duan, 2014). These three global models are based on empirical descriptions and are fitted on large data sets. The complex and non-linear relation between chemical components, melt structure and viscosity prevents the use of a model approach based on physical principles. But advances in machine learning algorithms, specifically artificial neural networks (ANN), provide an alternative route to describe the composition–viscosity relation. Using a large database, ANNs can find highly non-linear mappings between input and and output without prior knowledge of the mathematical form of this connection (Aggarwal, 2018). Recently, Tandia et al. (2019) have shown the capabilities of ANN to accurately fit and predict melt η for a database of technical glasses. Based on this success, Cassar (2021) produced an ANN architecture with a plethora of input parameters to predict η of silicate melts, the ANN by Le Losq et al. (2021) predicts several physical outputs but is limited to compositions in the K_2O-Na_2O-Al_2O_3-SiO_2 system. These studies use grey box approaches for the viscosity calculation, by predicting input parameters of certain viscosity equations (e.g., VFT or MYEGA) which are then used to compute η. This approach permits a physical interpretation of the predictions, within the constraints of the model.

However, with a scarcity of η data, this approach cannot be used for volcanic melts. The problem of sparse data is even more pronounced when considering the effect of water on η (Duan, 2014; Hui & Zhang, 2007; Giordano et al., 2008). Therefore, we do not follow the previous ANN studies with a grey box approach, but use a black box to utilise as many data as possible; this approach maps the input (composition x and T, where we treat H_2O on equal footing with the oxide components) directly to viscosity. We train an ANN using a database of viscosities for volcanologically relevant melts which we collected from the literature. We use 3482 data points from 153 data sets (not counting the variable H_2O content) for melts covering virtually the entire compositional space of magmas on Earth and some analogues of extraterrestrial melts (Figure 1). We show that the ANN is not only capable of fitting given data, but also of predicting η with high accuracy for the viscosity ranges in which measurements are performed.

To generate models that inter- and extrapolate in a physically sound way, which cannot be guaranteed using the black box approach, we combine the ANN with a "synthetic data" approach: For a composition of interest, we generate sets of η–T values from an ANN in two distinct η intervals in which viscosity measurements can be performed either by concentric cylinder or micropenetration/parallel plate viscometry (low viscosity, Lη, range: 10^{-3} Pa s $< \eta <$ 10^5 Pa s and high viscosity, Hη, range: 10^8 Pa s $< \eta < 10^{13}$ Pa s). These isochemical η values are then fit using the MYEGA equation (Mauro et al., 2009) for T dependence. Our approach combines the accuracy of the neural network trained on a large data set of η values and the physical basis of the MYEGA equation. An application/calculator of our model is available at `https://share.streamlit.io/domlang/visc_calc/main/final_script.py` (code and model can be found at `https://github.com/DomLang/Visc_Calc`).

2 Artificial Neural Networks

Artificial neural networks broadly refer to algorithms for pattern recognition, and here we make use of a simple architecture called a dense feed-forward multilayer perceptron (Aggarwal, 2018). It consists of three layer types: input, hidden and output (Figure 2). The layers contain so-called neurons, each storing a single numerical value. Each neuron of a layer is connected to every neuron in the following layer, hence dense, and every connection has a weight associated with it. The neuron values are propagated along these connections, and the weights are optimised during the learning process, analogous to variable parameters when fitting an equation to data. The neurons of the input layer store the input data (Section 3.1) which are propagated through all neurons of the hidden layers until the output (η) is calculated. The output is compared to the corresponding measurement using a loss function (Abadi et al., 2015), for which we use the mean squared error (MSE). The loss function is minimised, going backwards through the network tuning the weights. Furthermore, non-linearity is added using so-called activation functions (Aggarwal, 2018) which can be applied to the values of each neuron before they are propagated further through the network. This way the hidden layers become a non-linear mapping between input and output.

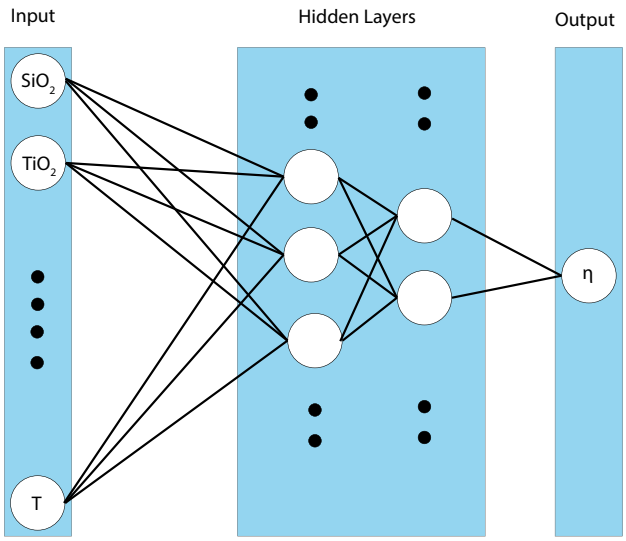

Figure 2. Sketch of a feed-forward multilayer perceptron. Circles are neurons storing single values. Each line connecting the neurons has a weight (regression parameter) and activation function associated with it. The black dots indicate that the number of neurons can hypothetically be arbitrary. The number of hidden layers can vary; here, we illustrate two layers used for our artificial neural network.

3 Database

We compile a database of 3482 tuples (T, x, η) for relevant melts from the literature. Of these, 2538 are data from measurements of only anhydrous samples, while 193 data sets with the remaining 942 data contain H_2O. The data span a large chemical domain in the total alkaline – silica (TAS) diagram (Figure 1). The database is separated into a training/validation (Table 1) and a test set (Table 2) with 3194 and 288 data points, respectively. The training/validation set contains 144 rock types which yield a total of 320 compositions, counting each H_2O content as a unique composition. Of these, 142 are anhydrous and 178 hydrous. The test set contains 15 rock types and again taking into account differing H_2O contents, 29 unique measured compositions. Of these, 14 are anhydrous and 15 hydrous data sets. The test sets are chosen such that they probe a reasonable chemical domain to check the reliability of the predictions made by the ANN.

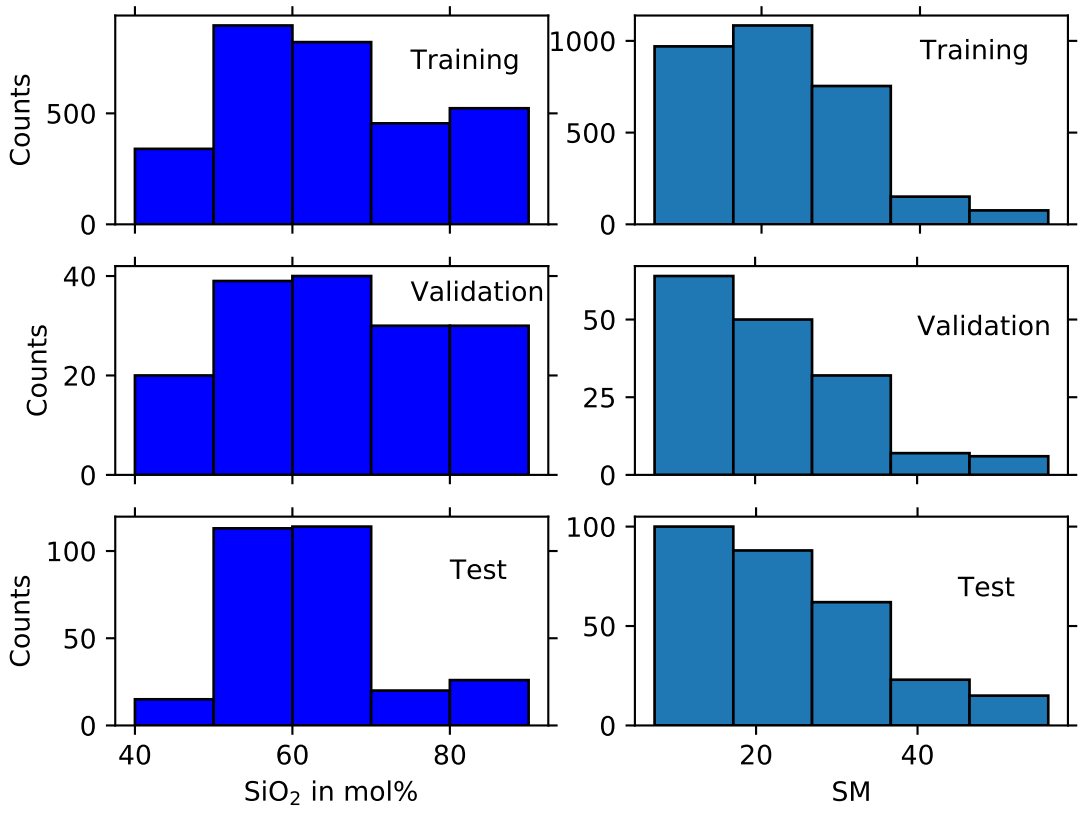

Figure 3. Histograms indicating the data distribution for one choice of the training, validation and test sets in terms of SiO_2 content (left column) and SM structural parameter (right column).

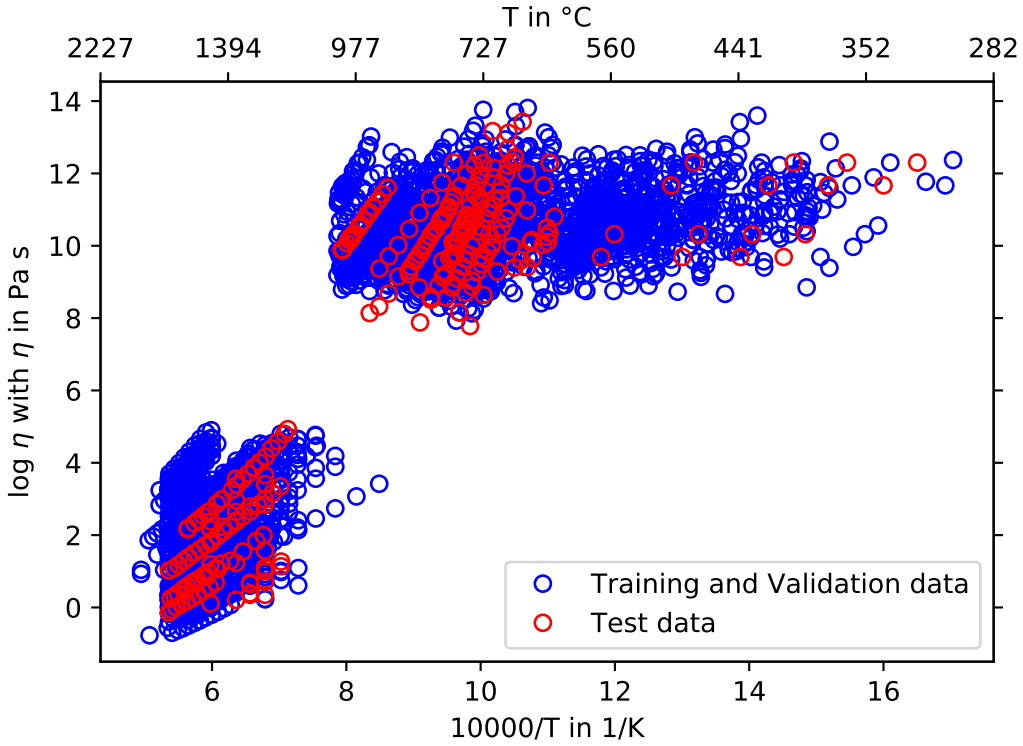

Figure 4. Viscosity ($\log \eta$) values from the data sets used here as a function of inverse temperature ($10000/T$). Data shown in blue are used in the training/validation process (Table 1), red crosses mark the test set (Table 2).

Silica content and the empirical parameter termed structure modifier content (SM, in mol%) (Giordano & Dingwell, 2003a) for one choice of the training and validation sets (Section 3.2) and for the test set are shown in Figure 3. The distributions for training and validation sets are very similar which indicates that the validation set tests the interpolation, not extrapolation, capabilities of a trained ANN. The SiO_2 content of data ranges from $\sim$ 37 wt% ($\sim$ 40 mol%) to $\sim$ 80 wt% ($\sim$ 85 mol%) and the H_2O content from 0 wt% to $\sim$ 6 wt% ($\sim$ 16 mol%). Measured η for Lη range from $\sim 10^{-1}$ to $\sim 10^{5}$ Pa s and for Hη from $\sim 10^{8}$ to $\sim 10^{14}$ Pa s. T spans approximately 1180 to 2020 K and 590 to 1270 K in the Lη and Hη range, respectively (Figure 4).

Table 1. Data sets used in the training and validation process, listed with decreasing SiO_2 content. Oxide compositions and H_2O are given in wt%. The H_2O content is given as the range found in the respective reference. TA = Na_2O + K_2O states the total alkali content (wt%). The first column gives the reference from which the data are taken, the last column indicates the sample name used in the respective publication. Detailed oxide compositions of the melts listed here are given in Table S1 in the Supporting Information as an Excel file.

Reference	SiO_2	TA	H_2O	Name in source	Reference	SiO_2	TA	H_2O	Name in source
(Hofmeister et al., 2014)	80.25	3.82		Moldavite	(Giordano et al., 2006)	60.71	4.42		MST
(Giordano et al., 2006)	79.43	3.91		MDV	(Giordano et al., 2000)	60.46	15.21	0.00-3.75	
(Le Losq & Neuville, 2013)	78.92	7.13		NAK83.8.0	(Giordano et al., 2009)	58.90	14.57		Mercato 1500
(Di Genova et al., 2017a)	78.87	6.29		F	(Giordano et al., 2009)	58.84	14.61	0.00-4.24	Mercato 1600
(Hess et al., 1995; Dingwell et al., 1996)	78.60	8.80	0.00-3.35	HPG8	(Whittington et al., 2001)	58.82	16.75	0.00-4.27	Phonolite
(Di Genova et al., 2017a)	77.86	6.39		G	(Giordano et al., 2009)	58.80	14.77		Mercato 1400
(Le Losq & Neuville, 2013)	77.82	8.99		NAK83.8.2	(Liebske et al., 2003)	58.69	4.87	0.00-1.96	Andesite
(Di Genova et al., 2017a)	77.63	6.06		A	(Vetere et al., 2006)	57.95	5.19	2.73	MD25
(Di Genova et al., 2017a)	77.56	7.15		C	(Vetere et al., 2006)	57.95	5.19	5.60	MD12
(Di Genova et al., 2017a)	77.28	6.32		B	(Robert et al., 2019)	57.32	15.27		Jd100
(Di Genova et al., 2017a)	77.25	7.58		H	(Robert et al., 2019)	57.12	17.92		Jd625
(Di Genova et al., 2017a)	76.83	7.22		D	(Sehlke & Whittington, 2015)	57.1	0.60		NVP
(Le Losq & Neuville, 2013)	76.81	10.00		NAK83.8.4	(Liebske et al., 2003)	56.65	4.79		Unzen-A
(Stabile et al., 2016)	76.62	9.71		Ebu-N-red	(Liebske et al., 2003)	56.65	4.79		Unzen-3
(Romine & Whittington, 2015)	76.53	8.50	0.00-0.34	NCA	(Liebske et al., 2003)	56.65	4.79		Unzen-2
(Stabile et al., 2016)	76.40	7.28		Ebu-N	(Liebske et al., 2003)	56.65	4.79		Unzen-4
(Di Genova et al., 2017a)	76.24	6.82		I	(Liebske et al., 2003)	56.65	4.79		Unzen-5
(Le Losq & Neuville, 2013)	76.10	10.75		NAK83.8.6	(Langhammer et al., 2021)	56.55	9.08	0.00-1.59	Lat-DSC
(Goto et al., 2005)	76.03	7.02	0.00-0.58		(Robert et al., 2019)	55.98	17.26		Jd75
(Stabile et al., 2016)	75.92	10.19		Ebu-B-red	(Robert et al., 2019)	55.86	19.79		Jd375
(Hess et al., 1995)	75.60	8.50		5Mg	(Robert et al., 2019)	54.85	18.81		Jd50
(Stabile et al., 2016)	75.39	11.28		Ebu-C	(Robert et al., 2019)	54.51	21.64		Jd0
(Di Genova et al., 2017a)	75.33	8.21		E	(Robert et al., 2013)	54.42	4.82	0.00-3.76	sba
(Stabile et al., 2016)	75.30	10.49		Ebu-B	(Giordano et al., 2009)	53.90	13.01		Pompei TR
(Stabile et al., 2016)	75.15	11.79		Ebu-C-red	(Giordano et al., 2006)	53.53	5.09		MRP
(Le Losq & Neuville, 2013)	75.11	11.70		NAK83.8.8	(Romano et al., 2003)	53.52	12.57	0.00-3.32	V_1631_W
(Hess et al., 1995)	74.60	13.60		5K	(Vetere et al., 2007)	53.47	8.38	0.00-4.75	Vul
(Friedman et al., 1963)	74.16	8.50	0.00-1.25		(Sehlke & Whittington, 2015)	53.3	0.35		IcP-HCT
(Hess et al., 1995)	74.10	13.40		5Na	(Romano et al., 2003)	53.14	13.05	3.07	V_1631_G
(Hess et al., 1995)	74.10	8.40		5Ca	(Robert et al., 2019)	53.12	20.64		Jd25
(Di Genova et al., 2017a)	73.75	6.72		J	(Robert, 2014)	53.08	4.76	0.00-2.92	fu18
(Whittington et al., 2004)	73.61	8.86	0.00-3.41	DK89	(Hofmeister et al., 2016)	53.08	4.76		Bas-and
(Stabile et al., 2016)	73.40	20.77		NFS-red	(Sehlke & Whittington, 2016)	53.02	3.23		CHW
(Hofmeister et al., 2014)	72.99	14.64		vase	(Sehlke & Whittington, 2016)	52.19	1.82		KREEPe
(Hofmeister et al., 2014)	72.91	15.71		1960	(Robert et al., 2015)	51.46	3.99	0.00-3.02	sb
(Hofmeister et al., 2014)	72.59	16.85		1895	(Sehlke & Whittington, 2016)	51.28	1.92		SHG
(Whittington, Bouhifd, & Richet, 2009)	72.31	9.49		HP96	(Giordano & Dingwell, 2003a)	51.20	11.65		Ves_W_tot
(Hofmeister et al., 2014)	72.19	3.62		Indoch	(Sehlke & Whittington, 2016)	50.65	0.35		KREEP
(Hess et al., 1995)	72.10	16.70		10Na	(Whittington et al., 2000)	50.56	10.05	0.00-2.27	Tephrite
(Di Genova et al., 2017a)	71.22	6.17		L	(Hofmeister et al., 2016)	50.40	2.79		P-MPRB
(Hess et al., 1995)	71.20	18.20		10K	(Hofmeister et al., 2016)	50.40	2.79		MORB
(Hess et al., 1995)	71.20	8.20		10Mg	(Misiti et al., 2009; Giordano et al., 2006)	50.17	4.63	0.00-4.16	SPZ, STB
(Hess et al., 1995)	70.60	8.20		10Ca	(Sehlke & Whittington, 2016)	50.06	3.51		Mu-Fe
(Langhammer et al., 2021)	70.50	9.90	0.00-3.55	Rhy14-DSC	(Sehlke & Whittington, 2016)	49.95	0.87		Lme
(Di Genova et al., 2013)	69.21	10.87	0.00-3.55	PS-GM	(Al-Mukadam et al., 2020)	49.90	0.00		Di
(Stabile et al., 2016)	69.14	24.61		NFS	(Sehlke & Whittington, 2016)	49.65	0.57		KOM
(Giordano et al., 2006)	68.80	10.19		CL_OF	(Robert et al., 2015)	49.40	3.70	0.00-2.7	fu06
(Le Losq & Neuville, 2013)	68.71	11.81		NAK75.12.0	(Giordano & Dingwell, 2003a)	49.20	9.20		Ves_G_tot
(Hofmeister et al., 2016)	68.41	7.02		Rhyo-dac	(Giordano et al., 2006)	49.07	4.83		STR
(Le Losq & Neuville, 2013)	68.28	12.49		NAK75.12.2	(Langhammer et al., 2021)	48.95	5.57	0.00-2.4	Bas1-DSC
(Le Losq & Neuville, 2013)	67.48	13.61		NAK75.12.5	(Giordano et al., 2009)	48.74	10.83		Pollena GM
(Le Losq & Neuville, 2013)	66.96	14.53		NAK75.12.7	(Giordano et al., 2009)	48.05	11.00		Pollena TR
(Le Losq & Neuville, 2013)	66.85	14.28		NAK75.12.6	(Morrison et al., 2019)	47.99	1.35		NOR
(Stabile et al., 2016)	66.26	27.28		KFS	(Giordano et al., 2009)	47.84	8.57	0.00-4.45	1906GM
(Giordano & Dingwell, 2003a)	66.00	6.00	0.00-1.98	UNZ	(Hofmeister et al., 2016)	47.45	4.01		OIB1
(Le Losq & Neuville, 2013)	65.75	15.80		NAK75.12.10	(Giordano & Dingwell, 2003b)	47.03	5.69	0.00-2.31	ETN
(Alidibirov et al., 1997)	65.28	5.63			(Sehlke & Whittington, 2016)	46.96	0.58		EUC
(Le Losq & Neuville, 2013)	64.90	16.40		NAK75.12.12	(Morrison et al., 2019)	46.91	1.78		ANOR
(Whittington et al., 2001)	64.45	10.07	0.00-4.92	Trachyte	(Sehlke & Whittington, 2016)	46.60	2.24		NAK
(Stabile et al., 2016)	64.44	27.56		KFS-red	(Morrison et al., 2019)	45.99	4.05		JSC-1a
(Hess et al., 1995)	64.30	26.20		20K	(Giordano et al., 2006)	45.76	3.72		SLP
(Hofmeister et al., 2016)	64.04	6.05		Dac-and	(Morrison et al., 2020)	44.76	7.19		NYI-1948
(Giordano et al., 2004)	63.88	12.49	0.00-3.86	MNV	(Whittington et al., 2000)	43.57	8.55	0.00-2.06	NIQ
(Hess et al., 1995)	63.20	7.50		20Mg	(Sehlke & Whittington, 2016)	42.16	0.52		LM
(Whittington, Hellwig, et al., 2009)	63.12	6.25	0.00-5.04	BRD	(Robert et al., 2019)	40.51	21.63		Ne100
(Hess et al., 1995)	62.90	7.40		20Ca	(Robert et al., 2019)	40.33	25.55		Ne625
(Richet et al., 1996)	62.40	4.45	0.00-3.46	Andesite	(Morrison et al., 2020)	39.61	10.61		NYI-1977
(Hess et al., 1995)	62.40	26.90		20Na	(Robert et al., 2019)	39.41	24.03		Ne75
(Romano et al., 2003)	61.26	12.62	0.00-3.78	AMS_B1	(Robert et al., 2019)	39.34	27.09		Ne375
(Neuville et al., 1993)	61.17	5.24		Andesite	(Sehlke & Whittington, 2016)	39.13	11.05		NYI
(Hellwig, 2006)	61.05	5.81	0.00-4.94	Dacite	(Robert et al., 2019)	37.87	26.18		Ne50
(Giordano et al., 2004)	60.74	11.60	0.00-3.41	IGC	(Robert et al., 2019)	37.28	27.51		Ne25

Table 2. Data sets used for testing the ANN, listed with decreasing SiO_2 content. Oxide compositions and H_2O are given in wt%. H_2O is given as the range found in the respective reference. TA = Na_2O + K_2O states the total alkali content (wt%). The first column gives the reference from which the data are taken, the last column indicates the sample name used in the respective publication. Detailed oxide compositions of the melts listed here are given in Table S2 in the Supporting Information as an Excel file.

Reference	SiO_2	TA	H_2O	Name in source
(Hofmeister et al., 2014)	79.63	8.59		Haplogranite
(Webb, 2021)	67.02	11.81		h16b
(Webb, 2021)	63.28	11.46		h22b
(Hofmeister et al., 2016)	62.16	5.84		Dacite
(Webb, 2021)	61.81	9.24		h5a
(Misiti et al., 2006)	59.90	12.55	0.18-5.81	AMS
(Langhammer et al., 2021)	57.72	11.62	0.00-4.78	Tra3-DSC
(Misiti et al., 2011)	56.08	8.88	0.00-3.28	FR
(Webb, 2021)	55.27	6.50		h34
(Sehlke & Whittington, 2015)	55.06	0.12		Enstatite Basalt
(Sehlke & Whittington, 2015)	55.02	6.47		NVP-Na
(Webb, 2021)	54.35	4.48		h10
(Hofmeister et al., 2016)	53.02	3.23		Dolerite
(Al-Mukadam et al., 2020)	49.90	0.00		Di, DSC derived viscosities
(Webb, 2021)	42.74	8.71		NIQ

3.1 General Data Preparation

In the training/validation set (Table 1) we initially consider anhydrous and hydrous data sets separately. They are each shuffled and then split into a training and validation set, according to ratios and procedures given in more detail in Section 3.2. The anhydrous and hydrous sets are then combined to finally yield training and validation sets containing both anhydrous and hydrous compositions. Since the number of hydrous data points is relatively small, this procedure ensures that there are sufficient hydrous data in the training set.

The input parameters and corresponding viscosity measurements of the training set are used for the regression during the learning process. After each learning cycle, the validation set is used to predict $\log \eta$. As these data have not been used to train the neural network, the validation set evaluates the ANN's ability to generalise, i.e., predict η. The loss function calculated from the validation set (validation loss) is also used to avoid overfitting. Overfitting is typically characterised as an increasing or constant validation loss, while the training loss keeps decreasing. This indicates that the ANN's ability to predict unknown values from input data remains constant or worsens despite an improving fit. The improvement in the fit is explained by the ANN learning the data by heart. This phenomenon can be mitigated using regularisation methods, such as dropout (Srivastava et al., 2014) which we use here (Section 3.2).

As input parameters, we use mole fractions of SiO_2, TiO_2, Al_2O_3, FeO, Fe_2O_3, MnO, MgO, CaO, Na_2O, K_2O, P_2O_5, H_2O, temperature T in K, the SM parameter (Giordano & Dingwell, 2003a) and the alkali ratio $K_2O/(K_2O+Na_2O)$. Contrary to the global viscosity models by Hui and Zhang (2007) and Giordano et al. (2008) that consider the iron content in the melt as FeO only, we differentiate between FeO and Fe_2O_3. This distinction is important as Fe_2O_3 acts as a network former, leading to an increase in melt vis-

cosity, while FeO acts as a network modifier, and has the opposite effect on viscosity (Dingwell & Virgo, 1987; Liebske et al., 2003; Bouhifd et al., 2004; Vetere et al., 2008; Chevrel et al., 2013; Kolzenburg et al., 2018; Stabile et al., 2021). For samples with only the total iron content FeO_{tot} reported, we distribute it evenly between FeO and Fe_2O_3 with a factor of 1.11 to account for the higher molar weight of Fe_2O_3 (Langhammer et al., 2021). SM reflects the effect of structural polymerisation on η, and the alkali ratio is known to significantly affect the viscosity of SiO_2-rich systems (Di Genova et al., 2017a; Le Losq & Neuville, 2013; Stabile et al., 2016). Cr_2O_3 is only used during the conversion from wt% to mole fractions. It is omitted during the training as the vast majority of compositions contain < 0.02 wt%.

To improve convergence and stability of the training process we scale the input data as follows (Montavon et al., 2012): (i) mole fractions of composition lie in the interval [0,1], (ii) T is normalised by dividing all values by the largest T within the data set (2023 K for Ne375, Table 1). (iii) We modify the definition of SM using mole fractions, also leading to values in the interval [0,1]. (iv) Finally for every value of each input parameter x_i the z-score (Cassar, 2021) is calculated as input according to

$$z_{i,j} = \frac{x_{i,j} - \mu_i}{\sqrt{\sigma_i^2}} \quad (1)$$

$$\mu_i = \frac{1}{N}\Sigma_{j=1}^{N} x_{i,j} \quad (2)$$

$$\sigma_i^2 = \frac{1}{N}\Sigma_{j=1}^{N}(x_{i,j} - \mu_i)^2 \; . \quad (3)$$

Here $x_{i,j}$ and $z_{i,j}$ denote the j-th value of the i-th input parameter (e.g., SiO_2 content), x denoting the old and z the z-score used as input for the ANN. μ_i is the average and σ_i^2 is the variance of the input. The scaling achieves an average of 0 and variance of 1 for the new input z_i. Values for μ and σ^2 can be found in Table S3 in the Supporting Information.

3.2 Training Procedure

Critical parameters for training an ANN (hyperparameters) are the number of hidden layers and neurons per layer which, through the associated weights, define the number of adjustable parameters, the learning rate which defines the step size during training, and the dropout value. The dropout randomly sets outputs of a layer to zero at a probability given by the dropout value. This simulates various different ANN's during a training session and reduces overfitting (Srivastava et al., 2014). As a measure for the quality of the ANN we use the root-mean-square-error (RMSE), commonly used in other publications. To search the space of hyperparameters, we use Bayesian optimisation as a stochastic algorithm (Aggarwal, 2018; Snoek et al., 2012) to find architectures with low validation errors. In this step, we perform the shuffling described above and combine 90% of the anhydrous and hydrous data sets each to the training set and the remaining 10% to the validation set.

In the Bayesian optimisation, we fix several hyperparameters: (i) We use two hidden layers. Several tests have shown little improvement when using three layers, and increasing the number of layers further increases the complexity which is not desired in our case given the scarcity of data. (ii) We apply the Adam optimiser (Kingma & Ba, 2014) as an algorithm, including the amsgrad flag (Reddi et al., 2019). (iii) For activation in all hidden layers we use the leaky ReLU function defined as

$$f(x) = \alpha x \quad \text{for } 0 > x, \quad (4)$$

$$f(x) = x \quad \text{for } 0 \leq x \; . \quad (5)$$

We use the default value of $\alpha = 0.3$ (Abadi et al., 2015). In the in- and output layers identity is used as activation. (iv) As batch size we use the complete training set (full batch).

For other hyperparameters we vary the range: (i) The number of neurons in the hidden layers explored are $1 - 256$ per layer, with final values of 256 for the first and 208 for the second layer. (ii) For the learning rate we use 0.057317962127906, after exploring $0.00001-0.5$. (iii) From a range of $0.0-0.5$, the chosen dropout value is 0.16569639948335368.

Using the ANN hyperparameters chosen by the Bayesian optimisation, we apply a 20-fold cross-validation process. All anhydrous and hydrous data sets in the training/validation database (Table 1) are shuffled separately and split into 20 sets each; one of each is combined to create 20 sets that contain anhydrous and hydrous data (superset). The ANN is trained 20 times, using 19 of the supersets for training and one as validation. The validation superset is exchanged until each superset was used for validation once. These architectures are used to predict all η values of the test set, and we present and discuss results for the ANN with the lowest RMSE.

Neural networks are built using TensorFlow (Abadi et al., 2015) and the Bayesian optimisation is performed with the KerasTuner (O'Malley et al., 2019), using Python as programming language. Data is managed and prepared using the Pandas and NumPy packages.

4 Training Results and Evaluation

The SiO_2 distribution for the training and validation set belonging to the network that displays the lowest RMSE when predicting the test set are very similar (Figure 3). Their RMSE values are 0.09 and 0.12, respectively (Figure 5). Therefore we expect the ANN to be trained to interpolate rather than extrapolate. This in turn leads us to recommend the use of this model only within the, albeit extensive, chemical bounds given by the training/validation data set (Figure 1). The models of Hui and Zhang (2007) and Giordano et al. (2008) applied to the training/validation sets in our database produce RMSE values of 1.36 and 1.18 respectively (Figure S1 in the Supporting Information).

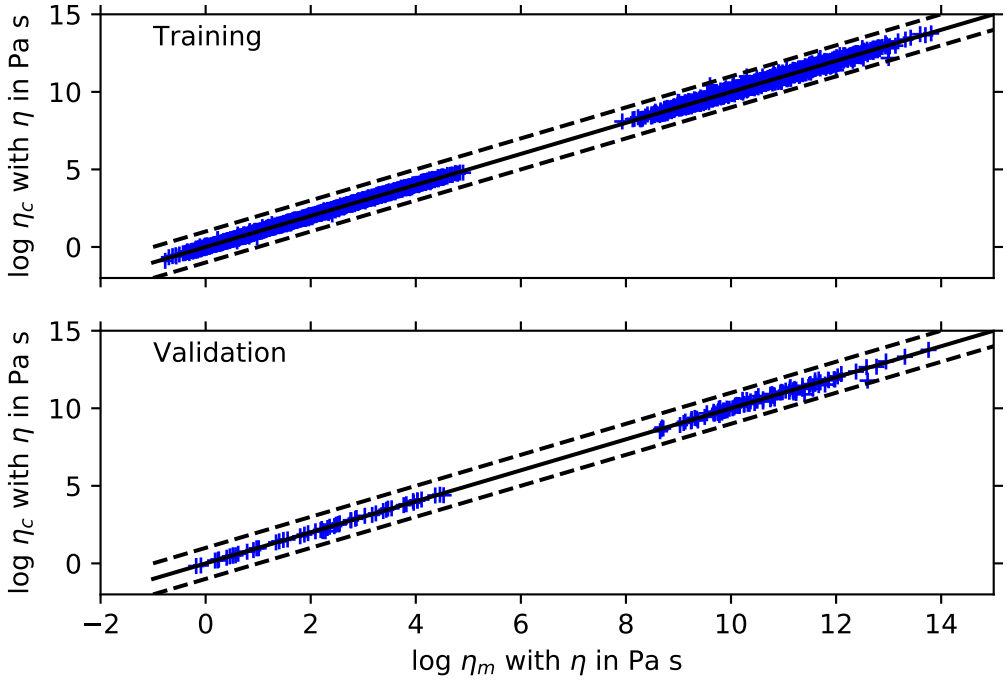

Figure 5. Calculated versus measured viscosities of the training (top) and validation sets (bottom) for the ANN yielding the lowest RMSE when applied to the test sets. The black solid line indicates the one to one correspondence, and dashed lines ±1 log-unit deviation from identity. RMSE values are 0.09 for the training and 0.12 for the validation set.

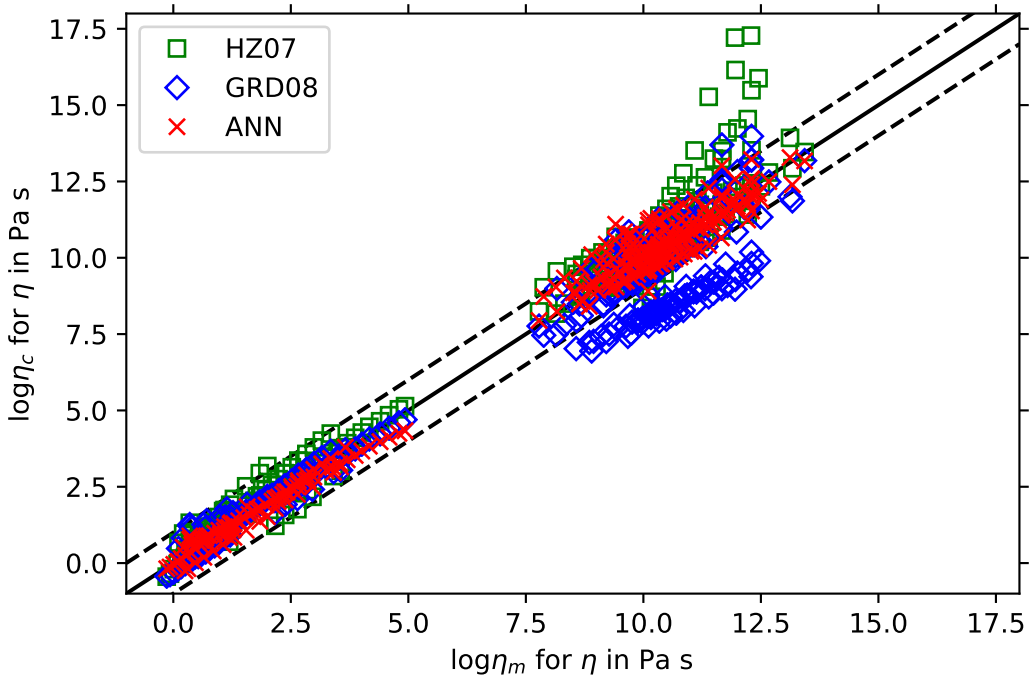

Figure 6. Comparison of measured and calculated viscosities for the artifical neural network (ANN, red crosses, RMSE = 0.45), the model by Giordano et al. (2008) (GRD08, blue diamonds, RMSE = 1.23) and Hui and Zhang (2007) (HZ07, green squares, RMSE = 0.89) for melts in the test sets. The one to one correspondence is shown by the solid black line, dashed lines indicate a ±1 log-unit deviation from identity.

For the test sets we compare measured η to predictions of our ANN and the global models of Hui and Zhang (2007) and Giordano et al. (2008) in Figure 6. The ANN predictions show the lowest RMSE with 0.45, compared to 0.89 and 1.23 for the models by Hui and Zhang (2007) and Giordano et al. (2008), respectively.

Both literature models show significantly larger deviations than the ANN prediction for specific data sets. The model by Hui and Zhang (2007) overestimate viscosity measurements for the enstatite and a Na_2O-rich basalt (NVP-Na) by Sehlke and Whittington (2015) and for the diopside (Di) determined from calorimetry experiments by Al-Mukadam et al. (2020). The model by Giordano et al. (2008) underestimate viscosities for these samples as well as for a haplogranite (Hofmeister et al., 2014). The two compositions by Sehlke and Whittington (2015) – models for basalts on Mercury – show a high content in CaO and MgO as does the diopside by Al-Mukadam et al. (2020) (Table S2 in the Supporting Information), outside typical terrestrial compositions. It may therefore not be surprising that the models by Hui and Zhang (2007) and Giordano et al. (2008) fail to reliably predict their η, while the training/validation set of our ANN contains two similar compositions from Sehlke and Whittington (2015) and further planetary tholeiitic melts (Sehlke & Whittington, 2016).

The high η for the fully polymerised haplogranite by Hofmeister et al. (2014) is not reproduced well by the model of Giordano et al. (2008) which also shows a poor fit for a similar model haplogranite (HPG8) by Hess et al. (1995).

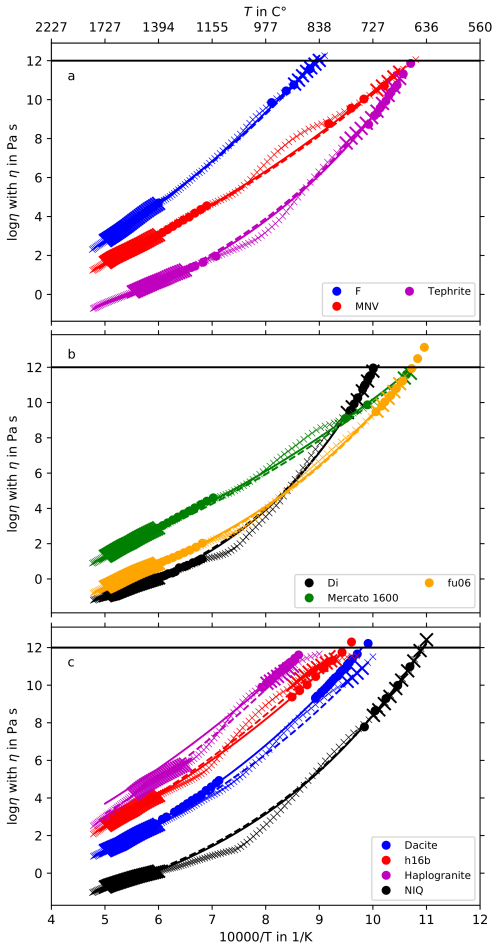

Figure 7. Viscosity ($\log \eta$) as a function of inverse temperature ($1000/T$) for some anhydrous compositions in the training/validation database (panels a and b) and the test set (panel c). Measurements are shown by filled circles, viscosity values predicted from the ANN by crosses, where bold crosses indicate the η range for the synthetic data approach. Solid (dashed) lines show MYEGA fits to the experimental (synthetic) data. Data references can be found in Tables 1 and 2. The horizontal lines indicate 10^{12} Pa s.

5 Synthetic Models

Eruptive temperatures of most magmas lie between the Hη and Lη range. At these temperatures, volcanic melts tend to crystallise faster then the timescale of the viscosity measurement. Therefore an interpolation – or extrapolation if data only exist at Hη – between these ranges is required to determine η. This is done by fitting η data using models, such as the MYEGA and VFT equations (Figure 7), sometimes modified to include a H_2O dependence. Contrary to MYEGA fits to experimental data, viscosities directly determined from the ANN in the range 10^5 Pa s $< \eta < 10^8$ Pa s show strong deviations from expected behaviour for some melt compositions (Figure 7). This is not surprising given the fact that the ANN is not trained in this η range due to the experimental gap discussed in the Introduction.

5.1 Creating a Synthetic Model

Mimicking the fitting of experimental data, we create a set of synthetic data from the ANN in the Hη and Lη ranges and fit the physically motivated MYEGA equation (Mauro et al., 2009)

$$\log \eta = A + (12 - A)\frac{T_\mathrm{g}}{T} \exp\left[\left(\frac{m}{12 - A} - 1\right)\left(\frac{T_\mathrm{g}}{T} - 1\right)\right] , \tag{6}$$

to them. The viscosity at infinite T, $A := \log \eta_\infty$, melt fragility m and glass transition temperature T_g (for $\log \eta = 12$) are fitting parameters. We fix $A = -2.9$, following our previous work and discussion (Langhammer et al., 2021), creating a two-parameter model equation for a specific composition that can be used to calculate η over a wide T range.

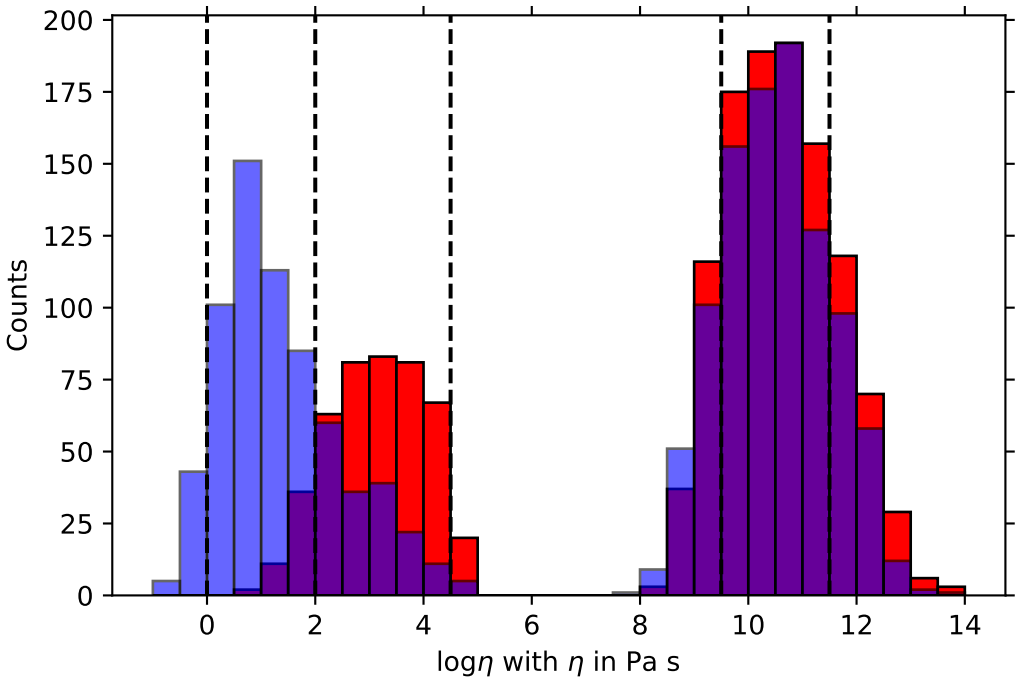

Figure 8. Distribution of viscosities in the training/validation database in the Hη and Lη regions, binned with $\log \eta = 0.5$ intervals. Data sets in both regions are split into compositions with $SiO_2 < 60$ wt% (blue) and $SiO_2 \geq 60$ wt% (red). Purple indicates the overlap of distributions. The vertical dashed lines indicate the $\log \eta$ ranges over which we create synthetic data, i.e., $[9.5, 11.5]$ at Hη for all compositions, and at Lη $[0, 2]$ or $[2, 4.5]$ for melts containing $SiO_2 < 60$ wt% and $SiO_2 \geq 60$ wt%, respectively.

Determining the Hη and Lη intervals for which synthetic data are created is an important step in the process, as this choice strongly influences the model parametrisation. We examine the distributions of $\log \eta$ for the whole database (Figure 8) to choose appropriate intervals for the Hη and Lη ranges. In the Hη region, the data density is the highest at $\log \eta$ between 10 and 11, and we create synthetic data in 1-log around the maximum, i.e., in the interval $[9.5, 11.5]$ with a step size of $\log \eta = 0.5$. Data coverage in the Lη region varies with SiO_2 content, and we split the data sets at 60 wt% SiO_2. With broad maxima for $\log \eta$ between 0.5 and 1.5 ($SiO_2 \leq 60$ wt%) and $\log \eta$ between 2.5 and 3.5 ($SiO_2 > 60$ wt%), we create synthetic data in the $\log \eta$ intervals $[0, 2]$ and $[2, 4.5]$,

respectively, again in steps of $\log \eta = 0.5$. Such a split is not necessary in the Hη range due to very similar distribution of data (Figure 8).

Technically, we use the ANN in conjunction with the bisection method to calculate T for the previously discussed $\log \eta$ values to a precision of 10^{-5}. The $\log \eta - T$ dependence is fit using the MYEGA model (equation 6 with $A = -2.9$). A web application which follows this scheme and calculates the MYEGA parameters and a viscosity value for a desired T can be found at `https://share.streamlit.io/domlang/visc_calc/main/final_script.py`. It is important to mention, that if the composition which is entered into the app only reports FeO_{total} one must split it according to $FeO = FeO_{total}/2$ and $Fe_2O_3 = FeO_{total}\frac{1.11}{2}$. On the other hand, if the compositions reports the total iron as Fe_2O_{3total} it must be split according to $FeO = \frac{Fe_2O_{3total}}{(2 \cdot 1.11)}$ and $Fe_2O_3 = Fe_2O_{3total}/2$. Fitting parameters m and T_g can be used for further calculations. An Excel table to calculate η values from the fit parameters m and T_g for various temperatures is supplied in the Supporting Information.

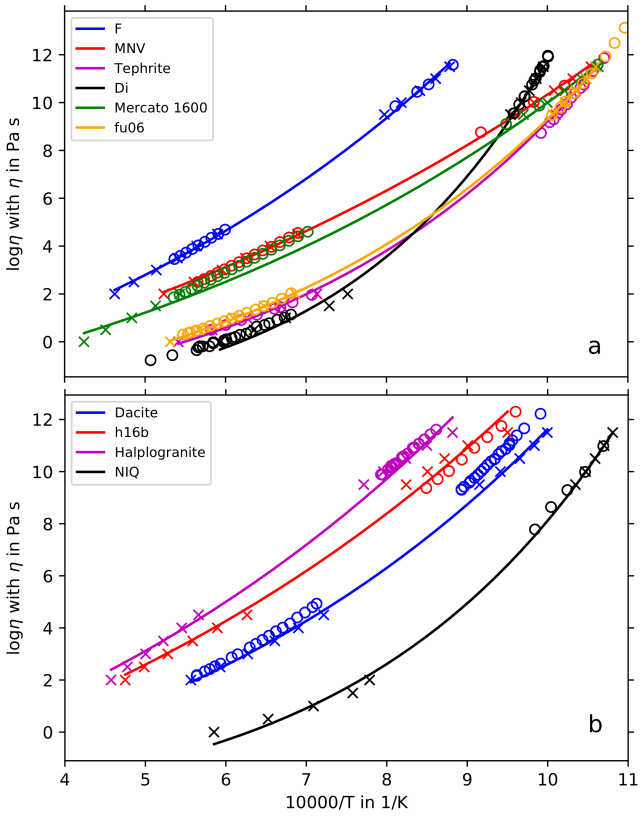

Figure 9. Comparison of fits to synthetic data to measurements for the compositions also used in Figure 7 (training/validation sets in panel a, test sets in panel b). Crosses are the synthetic data and lines are MYEGA fits (Mauro et al., 2009) to them. Circles are the respective measurements. Data references can be found in Tables 1 and 2.

5.2 Testing Synthetic Models

A comparison between the MYEGA fit to ANN viscosities (synthetic model) and direct experimental measurements for the compositions in the training/validation set (Figure 9a) already used in Figure 7 and discussed in Section 4 shows that the experimental measurements agree well with the ANN predictions where they overlap, both in the

Lη and Hη ranges. The synthetic fit describes the experimental T dependence of η measurements reasonably well, with the exception of Mercato 1600 (Giordano et al., 2009) that shows a more Arrhenian behavior in experiments. This discrepancy stems from the fact that, with an SiO_2 content of 58.84 wt%, the synthetic model is based on ANN viscosities in the $\log \eta$ interval $[0, 2]$, while experiments cover $\log \eta$ in a range 2−4.6. However, the direct ANN predictions reproduce measured η for Mercato 1600 quite well (Figure 7b).

A similar behaviour can be seen for samples from the test set in Figure 9b. The viscosity for three of the four compositions is described well, but values for the Dacite by Hofmeister et al. (2016) are predicted lower than the measurements by 0.9−0.7 log-units (decreasing with T) in the Hη range, while η of two Fe-free synthetic dacites in the training/validation set (Hellwig, 2006; Whittington, Hellwig, et al., 2009) is reproduced well. Evaluating the same compositions with the global model by Giordano et al. (2008) reveals that it has a similar problem predicting η for the Dacite by Hofmeister et al. (2016) although to a slightly smaller extent (0.7−0.5 log-units). As our model reproduces the experimentally measured η for the Dac-and by Hofmeister et al. (2016) with a similar iron content well, the reason for this specific discrepancy remains unclear.

The RMSE value for η in the training/validation set is 0.20 (Figure 10), slightly worse than those from the ANN directly (0.09 and 0.12 for training and validation, respectively). For the test set the values are 0.45 for the ANN predictions and 0.52 for the synthetic model, respectively. In comparison to RMSE values of 1.36 and 1.18 for the entire database by the global models of Hui and Zhang (2007) and Giordano et al. (2008), respectively, the synthetic model provides quite accurate results, and has a physical basis with the MYEGA equation.

The parameters for the MYEGA model (equation 6) do not differ significantly for T_g from the individual isochemical fits (Figures 11 and S2 in the Supporting Information) and the direct ANN inversion. For a reasonable comparison, only samples which include measurements in the Hη and Lη range from the training/validation set are included in Figures 11 and S2 in the Supporting Information. RMSE values of 18.3 K and 7.16 K for the direct ANN inversion and the synthetic model, respectively, reflect the narrow distribution in Figures 11 and S3 in the Supporting Information, and an average difference of $\delta T_g = -0.5$ K between the direct MYEGA fit and the synthetic model (Figure S2 in the Supporting Information) show that the synthetic model approach used here does not introduce any bias.

Values of melt fragility m derived from synthetic data tend to be slightly overestimated (Figure S3 in the Supporting Information), with the average deviation from direct MYEGA fits of $\delta\, m = 1.04$. A quasi-linear trend of increasing m with structural parameter SM discussed in Langhammer et al. (2021) is reproduced well.

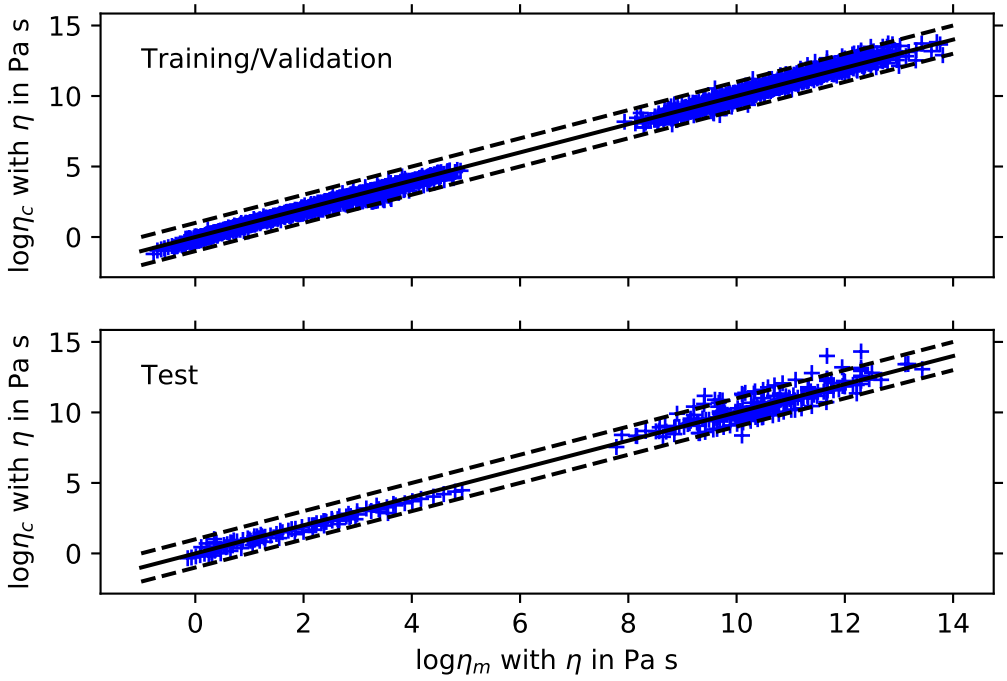

Figure 10. Comparison of viscosity values predicted by the synthetic models to measurements of the training/validation (top) and test (bottom) sets. The solid line shows the one to one correspondence, with the dashed lines ±1 log-unit deviations from identity. The respective RMSE values are 0.2 (top) and 0.52 (bottom).

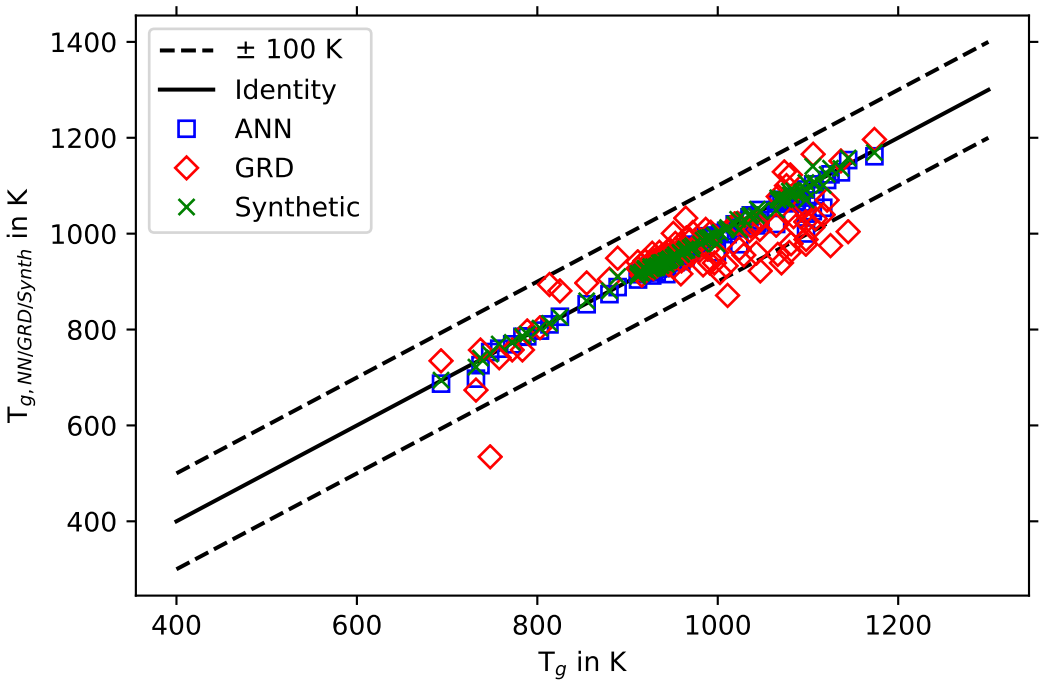

Figure 11. Comparison of calculated T_g values for compositions from the training/validation database. T_g on the x-axis are from isochemical MYEGA fits of the experimental data, on the y-axis T_g calculated from the ANN directly (squares), from the synthetic data approach (crosses) and from the model of Giordano et al. (2008) (GRD, diamonds) are shown. Only samples with measurements in both the Lη and Hη ranges in Table 1 are used. RMSE values are 18.3 K for the ANN, 7.16 K for the fit to synthetic data, and 57.53 K for the GRD model.

6 Conclusion

In this work we have trained an artificial neural network (ANN) on a database containing 3194 temperature-dependent viscosity (η) measurements for volcanic melts spanning a large chemical domain, including extraterrestrial model systems. The neural network takes melt composition, H_2O content, temperature T, the chemical parameters SM, reflecting melt polymerisation, and the alkaline ratio $K_2O/(Na_2O + K_2O)$ as input to predict η. We show that the trained neural network describes the data in the database very well, significantly better than commonly used global models (Hui & Zhang, 2007; Giordano et al., 2008). In this context it is worth emphasising that – contrary to such models – the ANN relies on data only, and makes no assumption on the functional dependence of viscosity. As such, interactions between different compositional components are taken into account implicitly. This suggests that despite the relatively scarce viscosity data for volcanic melts the success of ANN previously demonstrated for technical glasses (Cassar, 2021; Tandia et al., 2019) can be transferred to volcanology. To facilitate an easy use of our trained ANN, we make an online viscosity calculator available at `https://share.streamlit.io/domlang/visc_calc/main/final_script.py`.

The lack of training data in an η range 10^5-10^8 Pa s for T characteristic for volcanic eruptions results in unphysical behaviour of η. We therefore combine the reliable ANN predictions of η in the ranges where training data is available at high and low viscosity with a fit using the MYEGA equation to achieve a physically sound interpolation for geologically relevant conditions. The relevant parameters can be calculated using the application mentioned in the previous paragraph. An Excel file to calculate viscosites

using these parameters and the MYEGA equation (Mauro et al., 2009) is supplied in the Supporting Information.

Creating more accurate and versatile neural networks for melt viscosity, and other properties in general, is only limited by the quality and quantity of data. The time-consuming task of guessing a model equation and assuming critical parameters for melt characteristics is partly eliminated, while physical behaviour of the melt is implicitly included in the modelling process. With more data and further analysis, these implicit physical relations may reveal themselves and lead to a better understanding on composition-structure-property relations. Our results hopefully encourage other researchers to further explore machine learning algorithms in the context of natural silicate melts and volcanology. Finally, our model supports studies for numerical modelling of eruption scenarios and thus forecasting volcanic eruptions on a probabilistic basis.

Acknowledgments

We acknowledges funding by Deutsche Forschungsgemeinschaft (DFG) to DDG (grant DI 2751/2-1) and GSN (STE1105/13-2 within the Research Unit FOR2440). References to all data used in this study are documented in Tables 1, 2, and compositions of the melts are tabulated in the Supporting Information as Excel files (Tables S1 and S2). A web application to calculate the fitting parameters and viscosites can be found at `https://share.streamlit.io/domlang/visc_calc/main/final_script.py`. The calculater code and trained model can be found at `https://github.com/DomLang/Visc_Calc`. An Excel file to calculate further viscosities from the MYEGA equation is included in the Supporting Information.

References

Abadi, M., Agarwal, A., Barham, P., Brevdo, E., Chen, Z., Citro, C., ... Zheng, X. (2015). *TensorFlow: Large-scale machine learning on heterogeneous systems.* Retrieved from `https://www.tensorflow.org/` (Software available from tensorflow.org)

Aggarwal, C. C. (2018). *Neural networks and deep learning.* Springer.

Alidibirov, M., Dingwell, D. B., Stevenson, R. J., Hess, K.-U., Webb, S. L., & Zinke, J. (1997). Physical properties of the 1980 Mount St. Helens cryptodome magma. *Bull. Volcanol.*, *59*, 103–111. doi: /10.1007/s004450050178

Al-Mukadam, R., Di Genova, D., Bornhöft, H., & Deubener, J. (2020). High rate calorimetry derived viscosity of oxide melts prone to crystallization. *J. Non Cryst. Solids*, *536*, 119992. doi: /j.jnoncrysol.2020.119992

Bouhifd, M. A., Richet, P., Besson, P., Roskosz, M., & Ingrin, J. (2004). Redox state, microstructure and viscosity of a partially crystallized basalt melt. *Earth Planet. Sci. Lett.*, *218*, 31–44. doi: /10.1016/S0012-821X(03)00641-1

Cassar, D. R. (2021). ViscNet: Neural network for predicting the fragility index and the temperature-dependency of viscosity. *Acta Materialia*, *206*, 116602. doi: /10.1016/j.actamat.2020.116602

Cassidy, M., Manga, M., Cashman, K., & Bachmann, O. (2018). Controls on explosive-effusive volcanic eruption styles. *Nat. Commun.*, *9*, 2839. doi: /10.1038/s41467-018-05293-3

Chevrel, M. O., Giordano, D., Potuzak, M., Courtial, P., & Dingwell, D. B. (2013). Physical properties of $CaAl_2Si_2O_8$–$CaMgSi_2O_6$–FeO–Fe_2O_3 melts: Analogues for extra-terrestrial basalt. *Chem. Geol.*, *346*, 93–105. doi: /10.1016/j.chemgeo.2012.09.004

Colucci, S., & Papale, P. (2021). Deep Magma Transport Control on the Size and Evolution of Explosive Volcanic Eruptions. *Frontiers in Earth Science*, *9*, 436. doi: /10.3389/feart.2021.681083

Di Genova, D., Kolzenburg, S., Wiesmaier, S., Dallanave, E., Neuville, D. R., Hess,

K.-U., & Dingwell, D. B. (2017a). A compositional tipping point governing the mobilization and eruption style of rhyolitic magma. *Nature*, *552*, 235–238. doi: /10.1038/nature24488

Di Genova, D., Romano, C., Hess, K.-U., Vona, A., Poe, B. T., Giordano, D., ... Behrens, H. (2013). The rheology of peralkaline rhyolites from Pantelleria Island. *J. Volcanol. Geotherm. Res.*, *249*, 201–216. doi: /10.1016/j.jvolgeores.2012.10.017

Dingwell, D. B. (1996). Volcanic Dilemma–Flow or Blow? *Science*, *273*, 1054–1055. doi: /10.1126/science.273.5278.1054

Dingwell, D. B., Hess, K.-U., & Romano, C. (1998). Viscosity data for hydrous peraluminous granitic melts; comparison with a metaluminous model. *Am. Mineral.*, *83*, 236–239. doi: /10.2138/am-1998-3-406

Dingwell, D. B., Romano, C., & Hess, K.-U. (1996). The effect of water on the viscosity of a haplogranitic melt under PTX conditions relevant to silicic volcanism. *Contrib. to Mineral. Petrol.*, *124*, 19–28. doi: /10.1007/s004100050170

Dingwell, D. B., & Virgo, D. (1987). The effect of oxidation state on the viscosity of melts in the system Na_2O-FeO-Fe_2O_3-SiO_2. *Geochim. Cosmochim. Acta*, *51*, 195–205. doi: /10.1016/0016-7037(87)90231-6

Duan, X. (2014). A model for calculating the viscosity of natural iron-bearing silicate melts over a wide range of temperatures, pressures, oxygen fugacities, and compositions. *Am. Mineral.*, *99*, 2378–2388.

Friedman, I., Long, W., & Smith, R. L. (1963). Viscosity and water content of rhyolite glass. *J. Geophys. Res.*, *68*, 6523–6535. doi: /10.1029/JZ068i024p06523

Fulcher, G. S. (1925). Analysis of Recent Measurements of the Viscosity of Glasses. *J. Am. Ceram. Soc.*, *8*, 339–355. doi: /10.1111/j.1151-2916.1925.tb16731.x

Giordano, D., Ardia, P., Romano, C., Dingwell, D. B., Di Muro, A., Schmidt, M. W., ... Hess, K.-U. (2009). The rheological evolution of alkaline Vesuvius magmas and comparison with alkaline series from the Phlegrean Fields, Etna, Stromboli and Teide. *Geochim. Cosmochim. Acta*, *73*, 6613–6630. doi: /10.1016/j.gca.2009.07.033

Giordano, D., & Dingwell, D. B. (2003a). Non-Arrhenian multicomponent melt viscosity: a model. *Earth Planet. Sci. Lett.*, *208*, 337–349. doi: /10.1016/S0012-821X(03)00042-6

Giordano, D., & Dingwell, D. B. (2003b). Viscosity of hydrous Etna basalt: implications for Plinian-style basaltic eruptions. *Bull. Volcanol.*, *65*, 8–14. doi: /10.1007/s00445-002-0233-2

Giordano, D., Dingwell, D. B., & Romano, C. (2000). Viscosity of a Teide phonolite in the welding interval. *J. Volcanol. Geotherm. Res.*, *103*, 239–245. doi: /10.1016/S0377-0273(00)00226-2

Giordano, D., Mangiacapra, A., Potuzak, M., Russell, J. K., Romano, C., Dingwell, D. B., & Di Muro, A. (2006). An expanded non-Arrhenian model for silicate melt viscosity: A treatment for metaluminous, peraluminous and peralkaline liquids. *Chem. Geol.*, *229*, 42–56. doi: /10.1016/j.chemgeo.2006.01.007

Giordano, D., Romano, C., Papale, P., & Dingwell, D. B. (2004). The viscosity of trachytes, and comparison with basalts, phonolites, and rhyolites. *Chem. Geol.*, *213*, 49–61. doi: /10.1016/j.chemgeo.2004.08.032

Giordano, D., Russell, J. K., & Dingwell, D. B. (2008). Viscosity of magmatic liquids: a model. *Earth Planet. Sci. Lett.*, *271*, 123–134. doi: /10.1016/j.epsl.2008.03.038

Gonnermann, H. M., & Manga, M. (2007). The fluid mechanics inside a volcano. *Annu. Rev. Fluid Mech.*, *39*, 321–356. doi: /10.1146/annurev.fluid.39.050905.110207

Gonnermann, H. M., & Manga, M. (2013). Dynamics of magma ascent in the volcanic conduit. *Modeling volcanic processes: The physics and mathematics of volcanism*, 55–84.

Goto, A., Taniguchi, H., & Kitakaze, A. (2005). Viscosity measurements of hydrous rhyolitic melts using the fiber elongation method. *Bull. Volcanol.*, *67*, 590–596. doi: /10.1007/s00445-004-0401-7

Hellwig, B. M. (2006). *The viscosity of dacitic liquids measured at conditions relevant to explosive arc volcanism: determing the influence of temperature, silicate composition, and dissolved volatile content* (Unpublished doctoral dissertation). University of Missouri–Columbia.

Hess, K.-U., Dingwell, D. B., & Webb, S. L. (1995). The influence of excess alkalis on the viscosity of a haplogranitic melt. *Am. Mineral*, *80*, 297–304. doi: /10.2138/am-1995-3-412

Hofmeister, A. M., Sehlke, A., Avard, G., Bollasina, A. J., Robert, G., & Whittington, A. G. (2016). Transport properties of glassy and molten lavas as a function of temperature and composition. *J. Volcanol. Geotherm. Res.*, *327*, 330–348. doi: /10.1016/j.jvolgeores.2016.08.015

Hofmeister, A. M., Whittington, A. G., Goldsand, J., & Criss, R. G. (2014). Effects of chemical composition and temperature on transport properties of silica-rich glasses and melts. *Am. Mineral.*, *99*, 564–577. doi: /10.2138/am.2014.4683

Hui, H., & Zhang, Y. (2007). Toward a general viscosity equation for natural anhydrous and hydrous silicate melts. *Geochim. Cosmochim. Acta*, *71*, 403–416. doi: /10.1016/j.gca.2006.09.003

Kingma, D. P., & Ba, J. (2014). Adam: A method for stochastic optimization. *arXiv preprint arXiv:1412.6980*.

Kolzenburg, S., Di Genova, D., Giordano, D., Hess, K.-U., & Dingwell, D. B. (2018). The effect of oxygen fugacity on the rheological evolution of crystallizing basaltic melts. *Earth Planet. Sci. Lett.*, *487*, 21–32. doi: /10.1016/j.epsl.2018.01.023

Langhammer, D., Di Genova, D., & Steinle-Neumann, G. (2021). Modeling the Viscosity of Anhydrous and Hydrous Volcanic Melts. *Geochemistry, Geophys., Geosystems*, *22*, e2021GC009918. doi: /10.1029/2021GC009918

Le Bas, M. J., Le Maitre, R. W., Streckeisen, A., & Zanettin, B. (1986). A chemical classification of volcanic rocks based on the total alkali-silica diagram. *J. Petrol.*, *27*, 745–750. doi: /10.1093/petrology/27.3.745

Le Losq, C., & Neuville, D. R. (2013). Effect of the Na/K mixing on the structure and the rheology of tectosilicate silica-rich melts. *Chem. Geol.*, *346*, 57–71. doi: /10.1016/j.chemgeo.2012.09.009

Le Losq, C., Valentine, A. P., Mysen, B. O., & Neuville, D. R. (2021). Structure and properties of alkali aluminosilicate glasses and melts: insights from deep learning. *Geochim. Cosmochim. Acta*, *314*, 27–54. doi: /10.1016/j.gca.2021.08.023

Liebske, C., Behrens, H., Holtz, F., & Lange, R. A. (2003). The influence of pressure and composition on the viscosity of andesitic melts. *Geochim. Cosmochim. Acta*, *67*, 473–485. doi: /10.1016/S0016-7037(02)01139-0

Mauro, J. C., Yue, Y., Ellison, A. J., Gupta, K., & Allan, D. C. (2009). Viscosity of glass-forming liquids. *Proc. Natl. Acad. Sci. U.S.A.*, *106*, 19780–19784. doi: /10.1073/Proc.Natl.Acad.Sci.U.S.A..0911705106

Misiti, V., Freda, C., Taddeucci, J., Romano, C., Scarlato, P., Longo, A., ... Poe, B. T. (2006). The effect of H_2O on the viscosity of K-trachytic melts at magmatic temperatures. *Chem. Geol.*, *235*, 124–137. doi: /10.1016/j.chemgeo.2006.06.007

Misiti, V., Vetere, F., Freda, C., Scarlato, P., Behrens, H., Mangiacapra, A., & Dingwell, D. B. (2011). A general viscosity model of Campi Flegrei (Italy) melts. *Chem. Geol.*, *290*, 50–59. doi: /10.1016/j.chemgeo.2011.08.010

Misiti, V., Vetere, F., Mangiacapra, A., Behrens, H., Cavallo, A., Scarlato, P., & Dingwell, D. B. (2009). Viscosity of high-K basalt from the 5th April 2003 Stromboli paroxysmal explosion. *Chem. Geol.*, *260*, 278–285. doi: /10.1016/j.chemgeo.2008.12.023

Montavon, G., Orr, G., & Müller, K.-R. (2012). *Neural networks: tricks of the trade* (Vol. 7700). Springer.

Morrison, A. A., Whittington, A. G., Smets, B., Kervyn, M., & Sehlke, A. (2020). The rheology of crystallizing basaltic lavas from Nyiragongo and Nyamuragira volcanoes, DRC. *Volcanica*, *3*, 1–28. doi: /10.30909/vol.03.01.0128

Morrison, A. A., Zanetti, M., Hamilton, C. W., Lev, E., Neish, C. D., & Whittington, A. G. (2019). Rheological investigation of lunar highland and mare impact melt simulants. *Icarus*, *317*, 307–323. doi: /10.1016/j.icarus.2018.08.001

Neuville, D. R., Courtial, P., Dingwell, D. B., & Richet, P. (1993). Thermodynamic and rheological properties of rhyolite and andesite melts. *Contrib.to Mineral. Petrol.*, *113*, 572–581. doi: /10.1007/BF00698324

O'Malley, T., Bursztein, E., Long, J., Chollet, F., Jin, H., Invernizzi, L., et al. (2019). *Kerastuner.* `https://github.com/keras-team/keras-tuner`.

Papale, P. (1999). Strain-induced magma fragmentation in explosive eruptions. *Nature*, *397*, 425–428. doi: /10.1038/17109

Reddi, S. J., Kale, S., & Kumar, S. (2019). On the convergence of Adam and beyond. *arXiv preprint arXiv:1904.09237*.

Richet, P., Lejeune, A.-M., Holtz, F., & Roux, J. (1996). Water and the viscosity of andesite melts. *Chem. Geol.*, *128*, 185-197. doi: /10.1016/0009-2541(95)00172-7

Robert, G. (2014). The effects of volatiles on the viscosity and heat capacity of calc-alkaline basaltic and basaltic andesite liquids. *Doctoral Dissertation*(University of Missouri).

Robert, G., Knipping, J. L., Scherbarth, S., Robertson, T. E., Stechern, A., Behrens, H., & Whittington, A. G. (2015). Heat capacity and viscosity of basaltic melts with $H_2O \pm F \pm CO_2$. *Chem. Geol.*, *418*, 51–65. doi: /10.1016/j.chemgeo.2014.07.015

Robert, G., Smith, R. A., & Whittington, A. G. (2019). Viscosity of melts in the NaAlSiO4-KAlSiO4-SiO2 system: Configurational entropy modelling. *J. Non-Cryst. Solids*, *524*, 119635. doi: /10.1016/j.jnoncrysol.2019.119635

Robert, G., Whittington, A., Stechern, A., & Behrens, H. (2013). The effect of water on the viscosity of a synthetic calc-alkaline basaltic andesite. *Chem. Geol.*, *346*, 135–148. doi: /10.1016/j.chemgeo.2012.10.004

Romano, C., Giordano, D., Papale, P., Mincione, V., Dingwell, D. B., & Rosi, M. (2003). The dry and hydrous viscosities of alkaline melts from Vesuvius and Phlegrean Fields. *Chem. Geol.*, *202*, 23–38. doi: /10.1016/S0009-2541(03)00208-0

Romine, W. L., & Whittington, A. G. (2015). A simple model for the viscosity of Rhyolites as a function of temperature, pressure and water content. *Geochim. Cosmochim. Acta*, *170*, 281–300. doi: /10.1016/j.gca.2015.08.009

Sehlke, A., & Whittington, A. G. (2015). Rheology of lava flows on Mercury: An analog experimental study. *J. Geophys. Res. Planets*, *120*, 1924–1955. doi: /10.1002/2015JE004792

Sehlke, A., & Whittington, A. G. (2016). The viscosity of planetary tholeiitic melts: A configurational entropy model. *Geochim. Cosmochim. Acta*, *191*, 277–299. doi: /10.1016/j.gca.2016.07.027

Snoek, J., Larochelle, H., & Adams, R. P. (2012). Practical bayesian optimization of machine learning algorithms. *Advances in neural information processing systems*, *25*.

Srivastava, N., Hinton, G., Krizhevsky, A., Sutskever, I., & Salakhutdinov, R. (2014). Dropout: a simple way to prevent neural networks from overfitting. *J. Mach. Learn. Res.*, *15*, 1929–1958.

Stabile, P., Sicola, S., Giuli, G., Paris, E., Carroll, M. R., Deubener, J., & Di Genova, D. (2021). The effect of iron and alkali on the nanocrystal-free viscosity of volcanic melts: A combined Raman spectroscopy and DSC study. *Chem.*

Geol., *559*, 119991. doi: /10.1016/j.chemgeo.2020.119991

Stabile, P., Webb, S., Knipping, J. L., Behrens, H., Paris, E., & Giuli, G. (2016). Viscosity of pantelleritic and alkali-silicate melts: Effect of Fe redox state and Na/(Na+ K) ratio. *Chem. Geol.*, *442*, 73–82. doi: /10.1016/j.chemgeo.2016.09.003

Tammann, G., & Hesse, W. (1926). Die Abhängigkeit der Viskosität von der Temperatur bei unterkühlten Flüssigkeiten. *Z. Anorg. Allg. Chem.*, *156*, 245–257. doi: /10.1002/zaac.19261560121

Tandia, A., Onbasli, M. C., & Mauro, J. C. (2019). Machine learning for glass modeling. In *Springer handbook of glass* (pp. 1157–1192). Springer.

Vetere, F., Behrens, H., Holtz, F., & Neuville, D. R. (2006). Viscosity of andesitic melts—new experimental data and a revised calculation model. *Chem. Geol.*, *228*, 233–245.

Vetere, F., Behrens, H., Misiti, V., Ventura, G., Holtz, F., De Rosa, R., & Deubener, J. (2007). The viscosity of shoshonitic melts (Vulcanello Peninsula, Aeolian Islands, Italy): insight on the magma ascent in dikes. *Chem. Geol.*, *245*, 89–102. doi: /10.1016/j.chemgeo.2007.08.002

Vetere, F., Behrens, H., Schuessler, J. A., Holtz, F., Misiti, V., & Borchers, L. (2008). Viscosity of andesite melts and its implication for magma mixing prior to Unzen 1991–1995 eruption. *J. Volcanol. Geotherm. Res.*, *175*, 208–217. doi: /10.1016/j.jvolgeores.2008.03.028

Vogel, H. (1921). Das Temperaturabhängigkeitsgesetz der Viskosität von Flüssigkeiten. *Phys. Z.*, *22*, 645–646.

Webb, S. L. (2021). Viscosity of evolving magmas: a case study of the Glass House Mountains, Australia. *Bull. Volcanol.*, *83*, 1–12. doi: /10.1007/s00445-021-01495-8

Whittington, A. G., Bouhifd, M. A., & Richet, P. (2009). The viscosity of hydrous $NaAlSi_3O_8$ and granitic melts: Configurational entropy models. *American Mineralogist*, *94*, 1–16. doi: /10.2138/am.2009.2892

Whittington, A. G., Hellwig, B. M., Behrens, H., Joachim, B., Stechern, A., & Vetere, F. (2009). The viscosity of hydrous dacitic liquids: implications for the rheology of evolving silicic magmas. *Bull. Volcanol.*, *71*, 185–199. doi: /10.1007/s00445-008-0217-y

Whittington, A. G., Richet, P., Behrens, H., Holtz, F., & Scaillet, B. (2004). Experimental temperature–X(H_2O)–viscosity relationship for leucogranites and comparison with synthetic silicic liquids. *Earth Environ. Sci. Trans. R. Soc. Edinb.*, *95*, 59–71. doi: /10.1017/S0263593300000924

Whittington, A. G., Richet, P., & Holtz, F. (2000). Water and the viscosity of depolymerized aluminosilicate melts. *Geochim. Cosmochim. Acta*, *64*, 3725–3736. doi: /10.1016/S0016-7037(00)00448-8

Whittington, A. G., Richet, P., Linard, Y., & Holtz, F. (2001). The viscosity of hydrous Phonolites and Trachytes. *Chem. Geol.*, *174*, 209–223. doi: /10.1016/S0009-2541(00)00317-X

Supporting Information for "Modelling Viscosity of Volcanic Melts with Artificial Neural Networks"

D. Langhammer[1], D. Di Genova[1], G. Steinle-Neumann[1]

[1]Bayerisches Geoinstitut, Universität Bayreuth, 95440 Bayreuth, Germany

Contents of this file

1. Figures S1 to S3
2. Table S3

Additional Supporting Information (Files uploaded separately)

1. Captions for Datasets S1 (ds01) and S2 (ds02)

Introduction The Excel files contain information on the compositions used for training, validation and testing of the artificial neural networks. Figure S1 depicts the performance of literature models (Giordano et al., 2008; Hui & Zhang, 2007) on the training/validation dataset we compiled (Tables 1 and S1), Figures S2 and S3 show the behaviour of fit parameters T_g and m derived from our synthetic data approach compared to a direct fit. Table S3 contains the scaling parameters used in the input of the artificial neural network (Secton 3.1).

Data Set S1. The excel file ds01 includes two sheets. The sheet "wt%" contains the compositions of data used for training and validation in wt% of oxides and the base composition name from the respective reference. The sheet "mole frac input" contains the relevant input compositions in mole fractions (excluding Cr_2O_3 as it is not used to train the ANN) and the input parameters SM and $K_2O/(Na_2O + K_2O)$.

Data Set S2. The excel file ds02 includes two sheets. The sheet "wt%" contains the compositions of data used as test set in wt% of oxides and the base composition name from the respective reference. The sheet "mole frac input" contains the relevant input compositions in mole fractions (excluding Cr_2O_3 as it is not used to train the ANN) and the input parameters SM and $K_2O/(Na_2O + K_2O)$.

References

Giordano, D., Russell, J. K., & Dingwell, D. B. (2008). Viscosity of magmatic liquids: a model. *Earth Planet. Sci. Lett.*, *271*, 123–134. doi: /10.1016/j.epsl.2008.03.038

Hui, H., & Zhang, Y. (2007). Toward a general viscosity equation for natural anhydrous and hydrous silicate melts. *Geochim. Cosmochim. Acta*, *71*, 403–416. doi: /10.1016/j.gca.2006.09.003

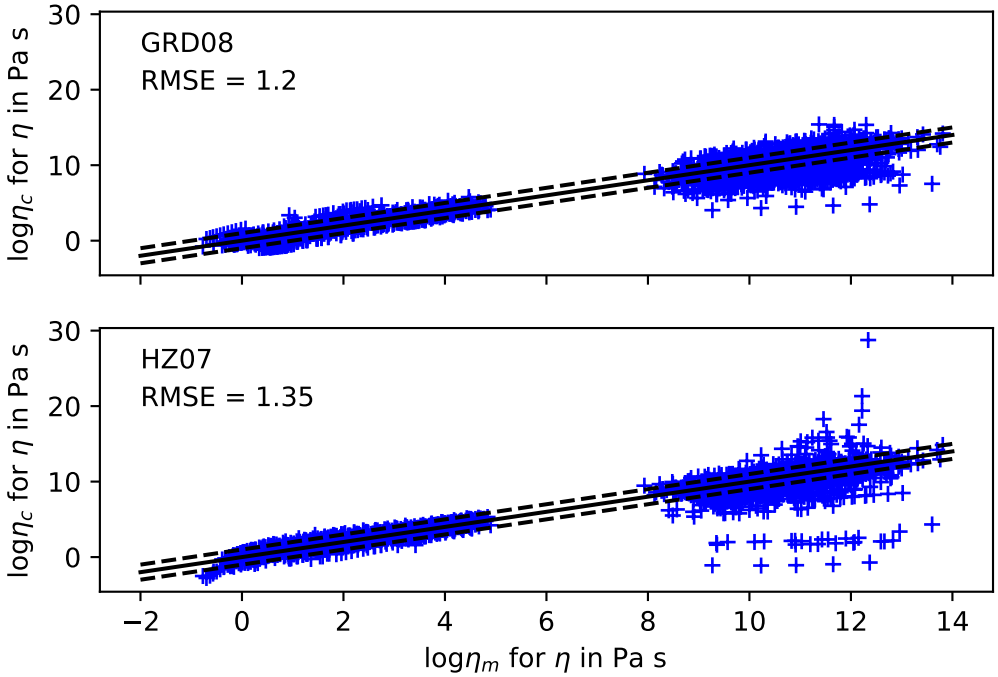

Figure S1. Comparison of calculated and measured viscosities for the models by Giordano et al. (2008) (top, GRD08) and Hui and Zhang (2007) (HZ07, bottom), when applied to the training and validation set (Table 1). The solid black line indicates the identity while the dashed lines give a deviation of ±1 log units.

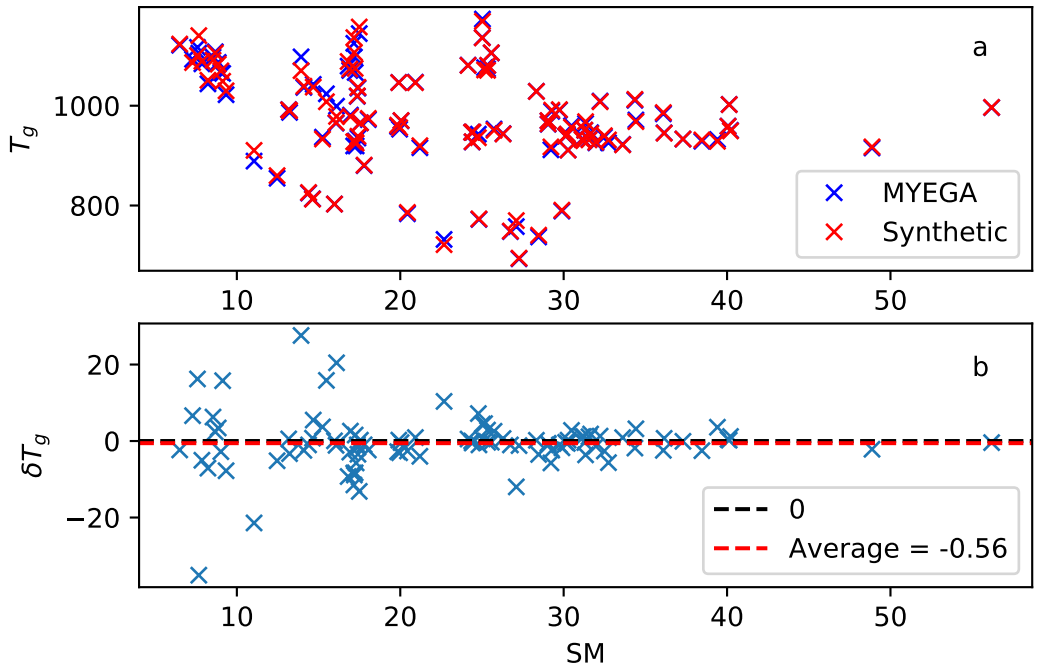

Figure S2. Comparison of T_{g} derived from direct fits to data and predictions using the synthetic data approach. Only data that include measurements in the Lη and Hη regime from the training/validation set are used. The top panel (a) shows T_{g} values from direct MYEGA fits (blue) and the synthetic model (red) plotted against SM. The bottom panel (b) depicts the difference $\delta T_{\mathrm{g}} = T_{\mathrm{g,MYEGA}} - T_{\mathrm{g,synth}}$.

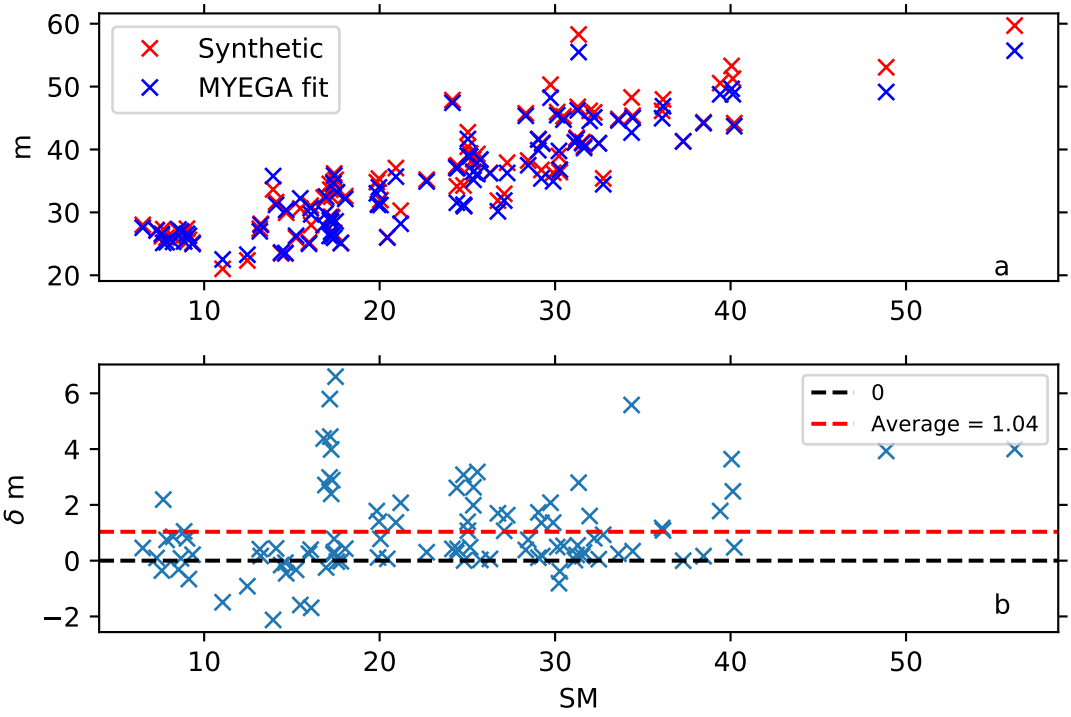

Figure S3. Comparison of m derived from direct fits to data and predictions using the synthetic data approach. Only data that include measurements in the Lη and Hη regime from the training/validation set are used. The top panel (a) shows m values from direct MYEGA fits (blue) and the synthetic model (red) plotted against SM. The bottom panel (b) depicts the difference $\delta m = m_{\mathrm{MYEGA}} - m_{\mathrm{synth}}$.

Table S3. Parameters μ and σ^2 for scaling of input data used for training/validation of the ANN.

Parameters	T	SiO_2	TiO_2	Al_2O_3	FeO	MnO	MgO	CaO	Na_2O	K_2O	P_2O_5	Cr_2O_3	Fe_2O_3	H_2O	SM	K/(Na+K)
μ	0.602848	0.646069	0.006122	0.105031	0.015038	0.000715	0.05675	0.06878	0.048986	0.028348	0.000494	6.37E-05	0.008792	0.014477	0.218617	0.324061
σ^2	0.031535	0.013967	7.55E-05	0.001869	0.000335	7.07E-07	0.004981	0.003721	0.001487	0.00103	1.63E-06	9.68E-08	0.000148	0.000994	0.010378	0.047454